Synthesis, Characterization, and Interlayer Distance Study of Zirconium Phosphonates with Stoichiometric Variation of Methyl and *p*-Aminobenzyl Pendant Groups

Willem R. Leenstra* and Jay C. Amicangelo

Department of Chemistry, University of Vermont, Burlington, Vermont 05405

Received June 15, 1998

A new class of layered zirconium mixed phosphonates, zirconium (*p*-aminobenzyl)phosphonate methylphosphonate, $Zr(O_3PCH_2C_6H_4NH_2)_x(O_3PCH_3)_{2-x}$ [abbreviated as $Zr(pab)_x(me)_{2-x}$], and its intercalated hydrochloride form, $Zr(O_3PCH_2C_6H_4NH_3Cl)_x(O_3PCH_3)_{2-x}$ [$Zr(pabHCl)_x(me)_{2-x}$], in a number of stoichiometric pendant group ratios, have been synthesized and characterized. For these materials, thermogravimetric analysis was able to identify and quantify, when present, loss of surface-adsorbed water, HCl units, methyl and *p*-aminobenzyl groups. ^{31}P NMR indicated evidence of two types of phosphorus environments that tracked the stoichiometry but behaved differently in chemical shift variation (6.7−8.5 and 2.2−8.0 ppm). FT-IR measurements quantitatively accounted for relative mole fraction as the pendant group ratio was varied. Interlayer spacing measurements as a function of the stoichiometric ratio were carried out by XRD and corroborated by molecular mechanics calculations. The calculations show that interlayer pendant group conformations (rotations about the anchoring P−C bond and of the benzenoid ring) are responsible for *d*-space variational behavior. It is observed that while Vegard's law is obeyed to some extent, deviation from linearity can be understood in terms of packing forces.

Introduction

Zirconium phosphate, $Zr(O_3POH)_2CH_2O$, is a layered solid whose structure was first determined by Clearfield.[1] Alberti[2] and Dines[3] later demonstrated that a related family of compounds known as zirconium phosphonates, $Zr(O_3PR)_2$, which also possess a layered structure can be synthesized using phosphonic acids instead of phosphoric acid. In these materials, the attractive interactions of the R groups that project into the interlayer region are responsible for stacking the zirconium planes.

It was subsequently shown that mixed zirconium phosphonates, $Zr(O_3PR)_x(O_3PR')_{2-x}$, can be formed by coprecipitation of the zirconium in the presence of two different phosphonic acids.[4−7] If the two organic groups on the phosphonic acids are sufficiently different in size, a material possessing interesting structural features may result. Zirconium phosph(on)ates are showing promise as useful new materials with applications in a variety of areas, such as catalysis,[8,9] ion exchange,[10] and photophysics.[11] A thorough review of metal phosphonate chemistry has recently appeared[12] and attests to the growth of this field of solid-state inorganic chemistry.

These mixed compounds usually contain a random mixture of the organic groups, i.e., a "solid solution" with all layers of identical stoichiometry. Several reports[13,14] have attempted to describe the changes in the magnitude of the interlayer spacing (*d* spacing) as a function of composition in terms of Vegard's law,[15] which states that the unit cell dimensions of mixed-metal solid solutions is a linear function of mole fraction, with the dimensions of the pure materials as the limits. However, the interpretation of the results is not totally unambiguous in that the scarcity of data points has also allowed an interpretation of certain mixed compounds exhibiting a stepwise dependence of interlayer spacing on concentration.[14] Under this interpretation, Vegard's law is violated.

In view of the above considerations, we undertook this investigation to (i) clearly establish whether Vegard's law holds for inorganic, layered systems and (ii) identify what physical/chemical attributes underlie its one-dimensional interlayer spatial variation.[16] Thus, in this work we have synthesized two new series of mixed zirconium phosphonates (with R as *p*-aminobenzyl and R′ as methyl) and characterized them in terms of their structural and chemical nature. We have also used molecular mechanics as a tool to better understand the details of the conformations of the organic pendant groups and how this affects the changes in the *d*-space values for the mixed derivatives.

Experimental Section

Materials and Instrumentation. $ZrOCl_2 \cdot H_2O$, (*p*-aminobenzyl)-phosphonic acid, methylamine, silicon (Aldrich), methylphosphonic acid

(1) Clearfield, A.; Smith, D. G. *Inorg. Chem.* **1969**, *8*, 431.
(2) Alberti, G.; Costantino, U.; Allulli, S.; Tomassini, N. *J. Inorg. Nucl. Chem.* **1978**, *40*, 1113.
(3) Dines, M. B.; DiGiacomo, P. M. *Inorg. Chem.* **1981**, *20*, 92.
(4) Dines, M. B.; DiGiacomo, P. M.; Callahan, K. P.; Griffith, P. C.; Lane, R. H.; Cooksey, R. E. In *Chemically Modified Surfaces in Catalysis and Electrocatalysis*; Miller, J. S., Ed; ACS Symposium Series; American Chemical Society: Washington, DC, 1982; p 223.
(5) Alberti, G.; Costantino, U.; Giuletti, R. *Gazz. Chim. Ital.* **1983**, *113*, 547.
(6) Alberti, G.; Costantino, U.; Kornyei, J.; Giovagnotti, M. L. *React. Polym.* **1985**, *4*, 1.
(7) Alberti, G.; Costantino, U.; Perego, G. *J. Solid State Chem.* **1986**, *63*, 455.
(8) Clearfield, A. *J. Mol. Catal.* **1984**, *27*, 251.
(9) Segawa, K.; Kihara, N.; Yamamoto, H. *J. Mol. Catal.* **1992**, *74*, 213.
(10) Alberti, G. *Acc. Chem. Res.* **1978**, *11*, 163.
(11) Vermeulen, L. A.; Thompson, M. E. *Chem. Mater.* **1994**, *6*, 77.
(12) Clearfield, A. In *Progress in Inorganic Chemistry*; Karlin, K. D., Ed.; Wiley: New York, 1998; Vol. 47, pp 371−510.
(13) Rosenthal, G. L.; Caruso, J. *Inorg. Chem.* **1992**, *31*, 3104.
(14) Rosenthal, G. L.; Caruso, J. *J. Solid State Chem.* **1993**, *107*, 497.
(15) Pearson, W. B. *The Crystal Chemistry and Physics of Metal Alloys*; Wiley: New York, 1972; p 174.
(16) Amicangelo, J. C.; Leenstra, W. R. *Abstracts of Papers*, 27th Northeast Regional Meeting of the American Chemical Society, Saratoga Springs, NY, 1997; American Chemical Society: Washington, DC, 1997; No. 174.

S0020-1669(98)00664-8 CCC: $15.00
Published on Web 09/18/1998

(Lancaster), hydrofluoric acid, and hydrochloric acid (J. T. Baker) were used as received.

X-ray diffraction (XRD) patterns were obtained with either a Philips PW1877 or a Scintag X1 automated powder diffractometer, using Cu Kα radiation and an internal silicon standard with all samples. Infrared spectra were recorded on a Perkin-Elmer System 2000 FT-IR instrument as KBr pellets. Thermogravimetric analysis (TGA) was performed on a Perkin-Elmer TGS-2 thermogravimetric analyzer interfaced to a System 7/4 console. All TGA scans were obtained using flowing compressed air and a 10 °C/min heating rate. ^{31}P solid-state NMR spectra were recorded on a Bruker ARX-500 500-MHz spectrometer (202.404 MHz for ^{31}P) using magic-angle spinning, ^{1}H high-power decoupling, and external referencing to 85% H_3PO_4. Molecular mechanics calculations were performed via the Cerius[2] modeling environment developed by Molecular Simulations Inc., using a modified version of its universal force field.

Zirconium Bis(methylphosphonate), $Zr(O_3PCH_3)_2$ [$Zr(me)_2$]. To a solution of zirconyl chloride (0.260 g, 0.805 mmol) in 18.4 mL of water was added 1.63 mL of 1.98 M HF (3.23 mmol). The resulting solution was added to a solution of methylphosphonic acid (0.155 g, 1.611 mmol) in 20.0 mL of water with stirring. The mixture was then refluxed under nitrogen for 6 days, after which the solution was cooled to room temperature and centrifuged. The precipitate was washed with water, acetone, and ether successively and air-dried to give $Zr(me)_2$ as a white solid (0.168 g, 75% yield).

Zirconium Bis[(*p*-aminobenzyl)phosphonate hydrochloride], $Zr(O_3PCH_2C_6H_4NH_3Cl)_2$ [$Zr(pabHCl)_2$], and Zirconium Bis[(*p*-aminobenzyl)phosphonate], $Zr(O_3PCH_2C_6H_4NH_2)_2$ [$Zr(pab)_2$]. A solution of zirconyl chloride (0.158 g, 0.491 mmol) in 5.0 mL of water was added dropwise to a solution of (*p*-aminobenzyl)phosphonic acid (0.184 g, 0.981 mmol) in 5.0 mL of 1.0 M HCl with stirring. An additional 30.0 mL of water was added to bring the total volume up to 40.0 mL, and the mixture was refluxed under nitrogen for 10 days. The solution was cooled to room temperature and centrifuged. The precipitate was washed successively with water, acetone, and ether and air-dried to give $Zr(pabHCl)_2$ as a beige powder (0.219 g, 84% yield). The hydrochloride salt was deprotonated by mixing the solid with a 2.0 M solution of methylamine in THF for 3−4 days under nitrogen. The suspension was then filtered, and the solid was washed with THF, water, acetone, and ether and air-dried.

Zirconium (*p*-Aminobenzyl)phosphonate Hydrochloride Methylphosphonate, $Zr(O_3PCH_2C_6H_4NH_3Cl)_x(O_3PCH_3)_{2-x}$ [$Zr(pabHCl)_x(me)_{2-x}$], and Zirconium (*p*-Aminobenzyl)phosphonate Methylphosphonate, $Zr(O_3PCH_2C_6H_4NH_2)_x(O_3PCH_3)_{2-x}$ [$Zr(pab)_x(me)_{2-x}$]. An identical synthetic procedure was followed for all of the mixed-stoichiometry compounds, $x = 0.25$, 0.5, 0.75, 1.0, 1.25, and 1.5. The following procedure is given for the $x = 1.0$ case, while for the other compounds the stoichiometric ratios of the two phosphonic acids were varied as necessary.

To a solution of (*p*-aminobenzyl)phosphonic acid (0.176 g, 0.938 mmol) and methylphosphonic acid (0.090 g, 0.937 mmol) in 10.0 mL of 4.3 M HCl was added, dropwise, a solution of zirconyl chloride (0.302 g, 0.938 mmol) in 10.0 mL of 1.0 M HCl with stirring. An additional 15.0 mL of water was added to bring the total volume up to 35.0 mL, and the mixture was refluxed under nitrogen for 19 days. Then 0.47 mL of 1.98 M HF (0.931 mmol) was added, and the solution was refluxed again for 7 days under nitrogen. The solution was cooled to room temperature, 30 mL of absolute ethanol was added, and the mixture was refrigerated to precipitate the solid. The solid was then filtered off, washed successively with 75% ethanol, acetone, and ether, and air-dried to give $Zr(pabHCl)_{1.0}(me)_{1.0}$ as a beige solid (0.356 g, 93% yield).

The hydrochloride salts were deprotonated by mixing the solid with a 2.0 M solution of methylamine in THF for 3−4 days under nitrogen. The resulting suspension was filtered, and the solid was washed with THF, water, acetone, and ether and air-dried.

For all compounds, spectral characterization and mass changes (described below) confirmed the predicted stoichiometries.

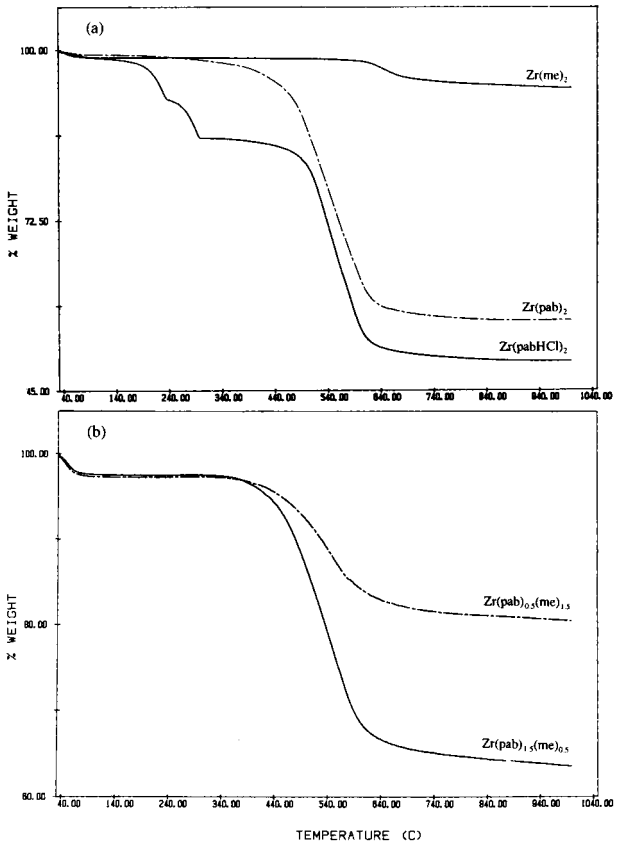

Figure 1. Thermogravimetric analysis curves of (a) $Zr(pabHCl)_2$, $Zr(pab)_2$, and $Zr(me)_2$ and (b) $Zr(pab)_{1.5}(me)_{0.5}$ and $Zr(pab)_{0.5}(me)_{1.5}$.

Results and Discussion

The series of mixed zirconium phosphonate compounds, $Zr(pabHCl)_x(me)_{2-x}$ and $Zr(pab)_x(me)_{2-x}$, will hereafter also be referred to as the protonated and deprotonated series, respectively. To investigate behavior across the full stoichiometric range, the value of x was varied from 0 to 2 in increments of 0.25 for both series. All materials were fully characterized by TGA and by IR and NMR spectroscopies. Structural parameters of the interlayer compounds were determined by XRD and subsequently corroborated by molecular modeling calculations.

Thermogravimetric Analysis. From the TGA results shown in Figure 1, panel a, it can be seen that $Zr(pabHCl)_2$ loses each HCl unit individually between 200 and 300 °C, followed by the fragmentation of *p*-aminobenzyl groups above 500 °C. The deprotonated $Zr(pab)_2$ shows only the volatilization of the *p*-aminobenzyl groups. A simpler result obtains for $Zr(me)_2$, which, in this particular sample, displays a loss of surface water below 100 °C, followed by pyrolysis of the methyl groups above 600 °C.

For the mixed derivatives, $Zr(pabHCl)_x(me)_{2-x}$ and $Zr(pab)_x(me)_{2-x}$, the two types of pendant moieties do not pyrolize discretely but instead volatilize together over a somewhat broadened range. Nevertheless, the change in percent weight loss for the various compounds with $x = 0.25$ to $x = 1.5$ conformed to the values predicted on the basis of relative pendant group stoichiometry and serves as one of our analytical confirmations. Figure 1, panel b, illustrates this quantitative behavior for two systems in the deprotonated series. We also observed that the protonated mixed series loses its HCl moieties at a lower temperature than does $Zr(pabHCl)_2$, indicating that in the mixed compounds the escape barrier has been lowered.

Infrared Spectroscopy. For all of the compounds synthesized in both the protonated and deprotonated series, one can see strong absorptions due to the stretching modes of the O_3P group between 1100 and 900 cm^{-1}. Also detectable for many of the samples are absorptions at 3430 and 1630 cm^{-1} which arise from the stretching and bending vibrations, respectively, of adsorbed water.

In the spectra of the compounds containing the *p*-aminobenzyl group, one sees a sharp, medium-intensity band arising from an aromatic ring mode at 1514 cm^{-1} for $Zr(pabHCl)_2$ and at 1520 cm^{-1} for $Zr(pab)_2$. The infrared spectrum of $Zr(me)_2$ lacks the IR signatures described above but clearly exhibits bands at 2993 and 2927 cm^{-1} due to methyl C−H stretching modes and a medium-intensity band at 1315 cm^{-1} which is attributed to the methyl bending modes.

The infrared spectra of the protonated systems show a very broad, strong band at 2841 cm^{-1}, indicative of the N−H stretch of a protonated amine, $R-NH_3^+Cl^-$, which is absent in the spectra of the deprotonated solids. The latter compounds display two bands at 3388 and 3313 cm^{-1}, attributed to the asymmetric and symmetric N−H stretches of the $R-NH_2$ group, respectively.

The uniformly changing composition of the mixed compounds can be quantified analytically via the infrared spectra of these mixed derivatives. In Figure 2, a pertinent section of the IR range is shown for the mixed solids in which *x* is varied from 0.25 to 1.50 in six steps. Quantitatively, the relative changes in the intensities of the bands at 1514 (aromatic) and 1315 cm^{-1} (methyl) track in a directly linear manner with stoichiometric parameter *x*.

NMR Spectroscopy. The solid-state ^{31}P NMR spectrum of $Zr(pabHCl)_2$ shows a single resonance at 7.99 ppm, while the spectrum of $Zr(pab)_2$ exhibits a resonance at 7.29 ppm. This observed shift upon deprotonation is as expected, since the lone pair on the nitrogen of the *p*-aminobenzyl group can now be involved in resonance structures that would add electron density to the ring and give rise to a shielding effect on the phosphorus atom.

Solid-state ^{31}P NMR can also be utilized to show the presence of two distinct phosphorus atoms in the mixed derivatives. Shown in Figure 3 are the NMR spectra for the protonated series, $Zr(pabHCl)_x(me)_{2-x}$. NMR spectra were obtained for the deprotonated series as well, but the two resonances for the methyl and *p*-aminobenzyl phosphorus atoms could not be resolved and therefore are not discussed further.

The NMR spectra for the protonated series clearly show two distinct phosphorus resonances, whose relative intensities can be seen to qualitatively change in accordance with the changes in stoichiometry. For phosphorus atoms attached to the methyl and to the *p*-aminobenzyl groups in the mixed series, the chemical shifts are given in Table 1. The chemical shift for the *p*-aminobenzyl phosphorus atoms in this series moves from 7.99 ppm for $Zr(pabHCl)_2$ to 2.18 ppm for $Zr(pabHCl)_{0.5}(me)_{1.5}$, while the resonance frequency for the methyl-attached phosphorus does not show a significant trend.

The observed shifting of the *p*-aminobenzyl ^{31}P resonances is believed to be due to conformational changes of the *p*-aminobenzyl group, which lead to changes in the magnetic environment of the phosphorus atom. From our molecular modeling studies (vide infra), it was found that when *x* is small (i.e., fewer bulky groups), a *p*-aminobenzyl group can attain a "fold-over" conformation and approach the zirconium plane to which it is attached more closely than when *x* is large. In turn, its minimum-energy geometry is such that the benzenoid ring

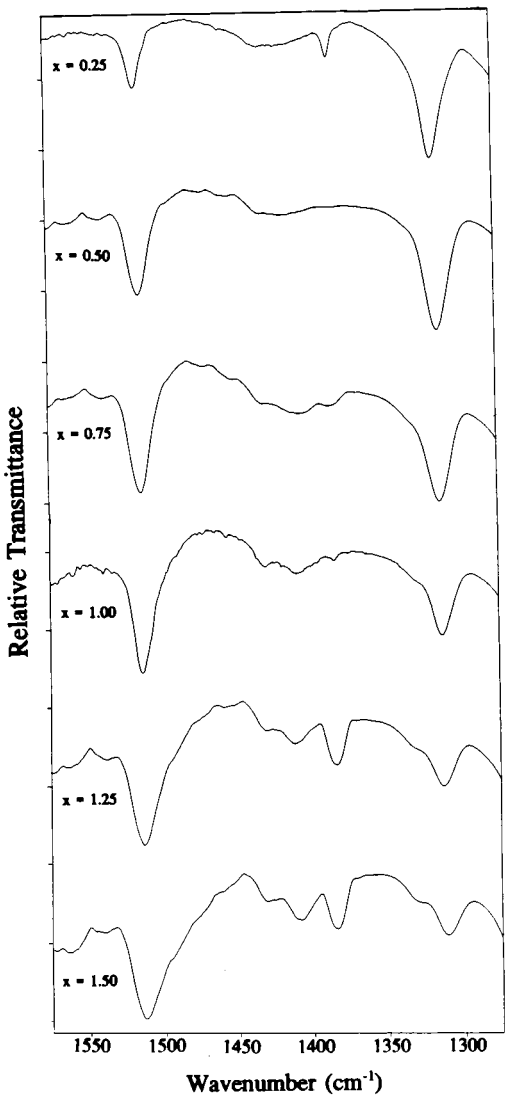

Figure 2. Infrared spectra of $Zr(pabHCl)_x(me)_{2-x}$ as a function of the stoichiometric parameter *x*. The band at 1514 cm^{-1} is attributed to the aromatic ring stretch, and the band at 1313 cm^{-1} is attributed to the methyl bending mode.

is allowed to rotate to a conformation in which it is more "parallel" to the zirconium plane than for the large-*x*, crowded systems. Conversely, in $Zr(pabHCl)_2$, the crowded nature of the interlayer forces the *p*-aminobenzyl moiety to adopt a "normal" conformation with respect to the zirconium planes, with benzenoid rings unavoidably "perpendicular" to the plane.

Given these calculated structural results, the phosphorus atom would be in a deshielding region of the ring current anisotropy for $Zr(pabHCl)_2$. As the relative number of methyl groups is increased, the benzene rings adopt the more parallel conformation with respect to the zirconium planes. This would then cause the phosphorus atom to be in a region more immediately above the benzene ring and experience a shielding effect due to ring current anisotropy. Therefore, it would be expected that the *p*-aminobenzyl phosphorus resonance would shift downfield with increasing number of *p*-aminobenzyl groups, as is observed. The data show that in the 1:1 compound the benzene ring has already arrived at its ultimate parallel conformation. The very slight chemical shift increase for the $x = 0.5$ compound appears to be a minor anomaly.

The methyl pendant group attached to the other type of phosphorus is not subject to any major conformational changes

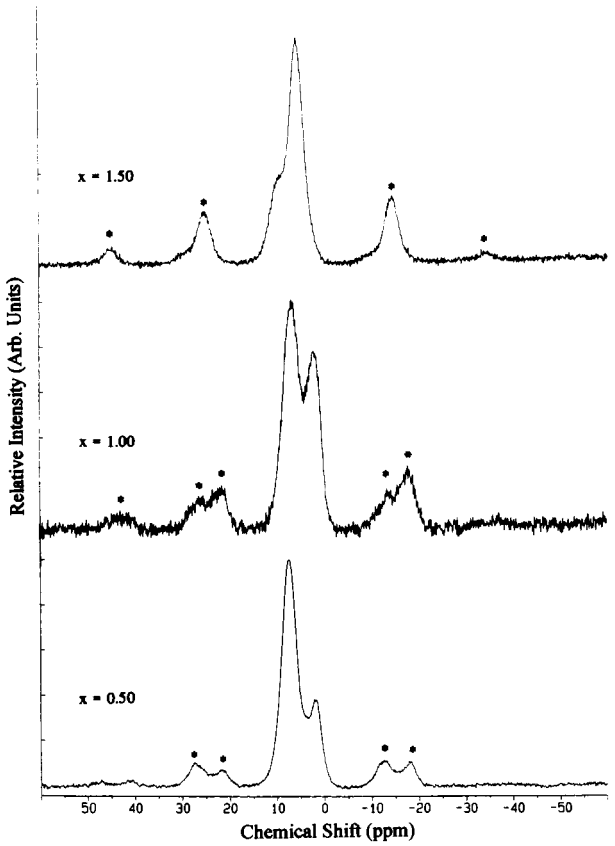

Figure 3. Solid state ^{31}P NMR spectra of $Zr(pabHCl)_x(me)_{2-x}$ for $x = 1.5$, $x = 1.0$, and $x = 0.5$. Spinning sidebands are marked with an asterisk.

Table 1. ^{31}P Chemical Shifts for $Zr(pabHCl)_x(me)_{2-x}$

compound	δ_{methyl} (ppm)	δ_{pabHCl} (ppm)
$Zr(pabHCl)_{2.0}$	–	7.99
$Zr(pabHCl)_{1.5}(me)_{0.5}$	8.52	5.43
$Zr(pabHCl)_{1.0}(me)_{1.0}$	6.65	2.03
$Zr(pabHCl)_{0.5}(me)_{1.5}$	7.57	2.18
$Zr(me)_{2.0}$	6.92	–

and therefore remains at a relatively constant chemical shift, as Table 1 shows.

X-ray Diffraction. A pure compound will exhibit a simple XRD pattern in which the scattering angle is a direct measure of the *d* spacing, via the Bragg equation. An example is provided in Figure 4, panel a, which illustrates the strong 001 line, followed by reduced intensities for higher order diffractions, for $Zr(pabHCl)_2$. For $Zr(me)_2$, panel c, the 001 diffraction line occurs at a much larger 2θ value, corresponding to a much smaller *d* spacing.

For a mixed compound where at least one of the components possesses a rotational degree or degrees of freedom, there are two different structural possibilities for distribution of the organic groups: (i) a random dispersion within the interlayer and all layers identical; (ii) an ordered segregation or staging of the organic groups into layers of distinct compositions. Each of these arrangements will give rise to characteristic features in the X-ray diffraction pattern. The randomly distributed structure will show a single 001 XRD peak whose *d* spacing is between the values observed for the two parent zirconium bis(phosphonates). On the other hand, the ordered, segregated structure will show a 001 reflection indicating a *d* spacing which is a sum of the *d*-space values for the two parent zirconium phosphonates. It should be noted that, for systems whose

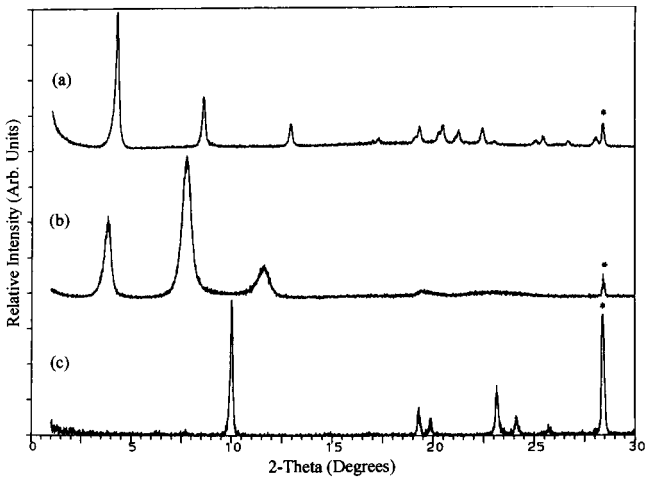

Figure 4. X-ray diffraction patterns of (a) $Zr(pabHCl)_2$, (b) $Zr(pabHCl)_{0.25}(me)_{1.75}$, and (c) $Zr(me)_2$. Trace b shows the presence of two compounds. One contains a randomly dispersed, indicated stoichiometric ratio of groups for all layers ($2\theta = 7.78°$). The second comprises two different, successively staged layers containing (i) all methyl groups and (ii) a 1:3 mixture of groups with a 2θ value of 3.83°. Peaks marked with an asterisk originate from the added standard, silicon powder.

interlayer constituents lack flexibility, *d*-space values of intermediate compounds may not lie between those of the parent compounds. For example, pillared systems where layers are held together covalently by a diphosphonate linkage exhibit a *d* spacing of the fully pillared system[17] even when an appreciable amount of pendant group derivatization is introduced.

Because of an unexpected anomaly, Figure 4, panel b, illustrates both types of mixed-system cases in one XRD trace. The most intense (second) diffraction line is indicative of the mixed zirconium phosphonate $Zr(pabHCl)_{0.25}(me)_{1.75}$, whose *d* spacing is intermediate in magnitude when compared to those of the parent compounds. The first diffraction peak, however, is seen to have a 2θ value even smaller than that of the all-pab compound and corresponds to an unusual, staged compound. (A discussion of this novel system follows in a later section.)

It can be seen from Figure 5 that for both series the interlayer spacing steadily escalates as the content of the larger pendant group is increased. After an initial, sharper rise between $x = 0.0$ and $x = 0.5$, an essentially linear increase is observed from $x = 0.5$ to $x = 1.5$. The increase in *d* spacing from $x = 1.5$ to bis(*p*-aminobenzyl) at $x = 2.0$ progresses with a reduced slope. For each deprotonated compound, the *d* spacing is consistently lower than that for the corresponding protonated species, but both series obey the same trend.

This type of behavior is in general agreement with Vegard's law, which predicts a linear change in lattice parameters with a change in composition for an ideal, solid solution. Therefore, it is believed that these compounds are randomly mixed zirconium phosphonates, in which the organic moieties are uniformly distributed within the interlayer region. However, the two breaks in each of the plots point to a clear deviation from strict linearity and from Vegard's law. Such behavior can only be understood from modeling studies, which can illuminate the steric factors that impact the interlayer distances.

Molecular Mechanics Calculations. Molecular modeling calculations were performed on selected stoichiometries in the $Zr(pab)_x(me)_{2-x}$ series, viz. where $x = 0.0$, 0.5, 1.0, 1.5, and

(17) Clearfield, A.; Wang, J. D.; Peng, G. Z. *Mater. Chem. Phys.* **1993**, *35*, 208.

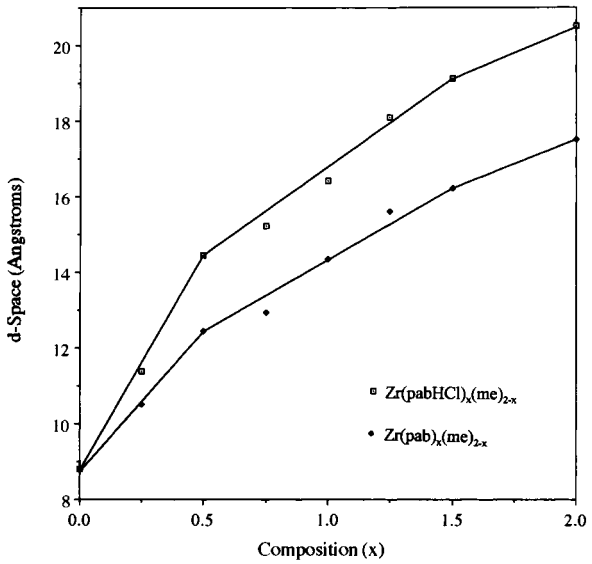

Figure 5. Variation in *d* spacing measured by XRD as a function of composition for $Zr(pabHCl)_x(me)_{2-x}$ and $Zr(pab)_x(me)_{2-x}$.

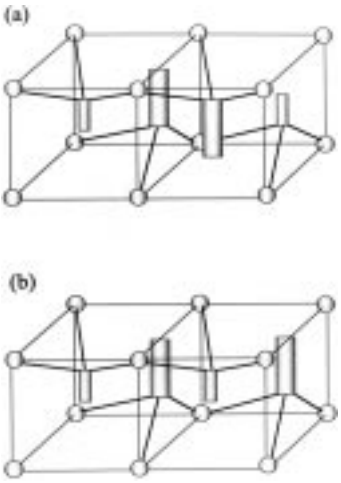

Figure 6. Schematic depictions of $Zr(pab)_1(me)_1$ unit cells in which the oppositely placed large groups are (a) at closest-approach distance and (b) at maximized separation from each other. The large and small columns represent respectively the *p*-aminobenzyl and the methyl groups.

Table 2. Molecular Mechanics *d*-Space Values for $Zr(pab)_x(me)_{2-x}$

compound	pab:me	d_{cal} (Å)	d_{obs} (Å)
$Zr(pab)_{2.0}$	4:0	18.1	17.5
$Zr(pab)_{1.5}(me)_{0.5}$	3:1	16.9	16.2
$Zr(pab)_{1.0}(me)_{1.0}$	2:2	14.4	14.4
$Zr(pab)_{0.5}(me)_{1.5}$	1:3	12.8	12.4
$Zr(me)_{2.0}$	0:4	9.4	8.8

2.0. The basic unit cell for all models, shown in Figure 6, consists of two zirconium atoms and four phosphonate sites. For each stoichiometry, a model was built using the appropriate numbers of *p*-aminobenzyl and methyl groups. Calculations were performed to find the global minimum, which was achieved by initiating a myriad of different *c*-axis starting distances (both larger and smaller than those of the ultimate structure) as well as relative conformations of the organic moieties. For each final, minimized model, the X-ray diffraction pattern was simulated and the *d* spacing was calculated. Table 2 lists these calculated results along with the experimental *d* spacings, for each stoichiometry.

As can be seen from Table 2 and Figure 7, the calculations

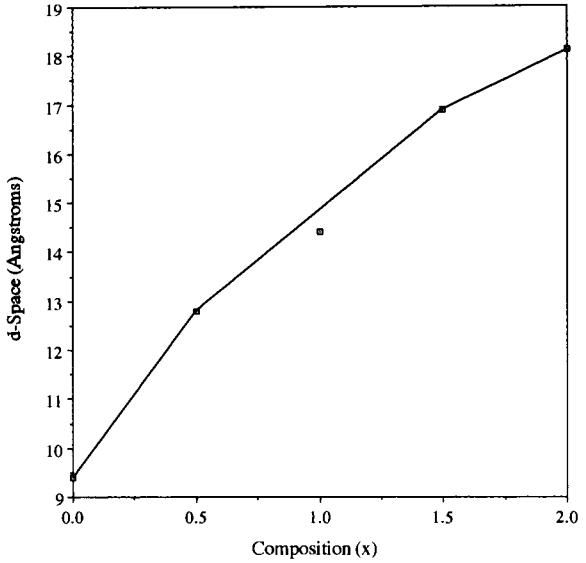

Figure 7. Variation in the calculated *d* spacing as a function of composition for the molecular mechanics energy-minimized models of $Zr(pab)_x(me)_{2-x}$.

predict a generally linear variation in the *d* spacing with changing composition, in agreement with the observed pseudo-Vegard's law type behavior displayed in Figure 5. It should be noted that the calculated *d* spacings are slightly higher than the experimental *d* spacings; this can be attributed to a systematic inaccuracy in the force field. Refinements of the force field that would provide an even better fit of the predicted geometrical features (in particular the *d* spacing) with those determined via its X-ray structure are currently in progress.

The modeling of the $Zr(pab)_1(me)_1$ compound presents a slight complication not present with the other stoichiometries, in that there are two possible ways in which to arrange the groups in their four unit-cell sites (excluding the higher-energy arrangement of pendant groups segregating on opposing sides of the interlayer). As can be seen from Figure 6 in panels a and b, respectively, the phosphonate moieties can be arranged such that the *p*-aminobenzyl groups pointing into the interlayer region from opposite planes are near one another or such that the pendant groups are configured with a *p*-aminobenzyl group nearest a methyl group. We have denoted these two different configurations as **2:2a** and **2:2b**, respectively.

Calculations were performed for each of these orientations, and their global minima were found to be only on the order of 1% different in energy. However, it was found that the *d* spacings of the minimum-energy structures for each were different: 14.4 Å for **2:2a** and 12.8 Å for **2:2b**. We believe that the *d* spacing for the **2:2a** model (14.4 Å) is a more realistic value, since in a compound with a statistical mix of **2:2a** and **2:2b** structures, there would be a sufficient number of *p*-aminobenzyl groups opposite/near one another to actually "prop up" the interlayer distance to the higher value.

Qualitatively, the changes in the *d* spacing with composition can be rationalized in terms of interrelated factors that pertain to the steric interactions of the bulkier *p*-aminobenzyl groups and the conformations of the organic groups. In a prototypical compound, zirconium phenylphosphonate,[2] the phenyl group's anchoring P−C bond is not normal to the zirconium plane but was found to be tilted[18] by 30°, close to the value for the $P-CH_2$ bond in our calculated structures. Because of the sp^3 nature of

(18) Poojary, D. M.; Hu, H. L.; Campbell, F. L., III; Clearfield, A. *Acta Crystallogr., Sect. B* **1993**, *49*, 996.

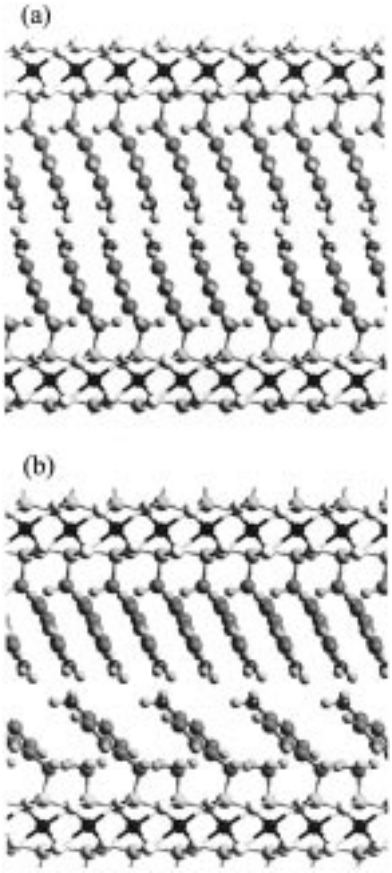

Figure 8. Molecular mechanics-generated structures of (a) $Zr(pab)_2$ and (b) $Zr(pab)_{1.5}(me)_{0.5}$.

the carbon atom, rotation about the P−C bond can point the *p*-aminobenzyl group toward the next layer (normal) or lay it down toward its own attachment layer (folded over). The normal conformation is associated with the crowded $x = 2.0$ compound and leads to a large interlayer distance. For a compound in which a given *p*-aminobenzyl group is surrounded by methyl groups, sterically directed energetics allow it to adopt the fold-over conformation to the extent allowed by the P−C rotation, with a concomitant adoption of a parallel conformation of the benzenoid ring with respect to the zirconium plane. Intermediate *x* values result in intermediate steric constraints, resulting in *d* values between the two extremes.

As can be seen in Figure 8, panel a, for $Zr(pab)_2$ the *p*-aminobenzyl groups are all in the normal, perpendicular conformation. Accordingly, the *d* spacing is calculated to be a large value of 18.1 Å for this model.

The model of $Zr(pab)_{1.5}(me)_{0.5}$, depicted in Figure 8, panel b, reveals that the *p*-aminobenzyl rings next to each other in the top layer will be in a normal conformation while the *p*-aminobenzyl group in the layer below is next to a methyl group and exists in a fold-over conformation. It should be noted that the three-dimensionally replicated unit cell, which is shown in Figure 8, panel b, is only a schematic representation of the real compound and should instead depict a randomization of the initial unit cell. Nevertheless, the *d* spacing is lowered as compared to that of $Zr(pab)_2$.

The calculated minimum-energy models for model **2:2a** of $Zr(pab)_1(me)_1$ and $Zr(pab)_{0.5}(me)_{1.5}$ predict that the *p*-aminobenzyl rings will be in successively more parallel conformations, and therefore the *d* spacings are lowered even further with respect to $Zr(pab)_2$ and $Zr(pab)_{1.5}(me)_{0.5}$. As expected, the all-methyl compound was found to possess the smallest *d* spacing value at 9.4 Å.

On the basis of these arguments, it is reassuring to note that the predicted *d*-space value for $Zr(pab)_1(me)_1$, in which there are only *p*-aminobenzyl groups in nearest opposite-neighbor positions relative to methyl groups (the **2:2b** model discussed earlier), is the same as that for $Zr(pab)_{0.5}(me)_{1.5}$.

Overall, the results of the calculations show a remarkable agreement between theory and experiment in two important aspects. First of all, the linear behavior in the midrange of stoichiometries was corroborated. Even more gratifying was the result that the modeling also accurately predicts a compression of the layers for the unmixed compounds at both ends of the stoichiometric variation, as was observed experimentally.

This compacting effect can be rationalized in that crystal packing forces act most effectively when only one type of molecule is involved. The XRD pattern (Figure 4) supports this point. When, in the pure compounds, packing forces act to produce a material of high crystallinity, XRD peaks are narrowed as compared to those of mixed compounds. Accordingly, the XRD peak of $Zr(pabHCl)_{0.25}(me)_{1.75}$ in panel b exhibits a line width approximately 3 times larger than those for the pure compounds depicted in panels a and c.

It appears that a strict carryover of Vegard's law from its origins in metallic alloys[15] to layered inorganic solids may not be appropriate.[19]

A Novel Staged Compound. As mentioned earlier, the XRD spectrum for the $x = 0.25$ protonated compound is shown in Figure 4, panel b. A similar result obtains for the deprotonated compound. The 001 (lowest angle) peak calculates, via the Bragg equation, to *d*-space values of 23.0 and 21.6 Å for these protonated and deprotonated series, respectively. Since these values are larger than the *d* spacings for the fully derivatized (with large groups) protonated (20.5 Å) and deprotonated (17.5 Å) compounds, these data can only be interpreted in terms of a structure in which the repeating unit consists of two different layers, i.e., a staged structure. Staged compounds in which the two alternating, different layers are each purely comprised of one pendant group have been observed before.[17,20−22] However, adding an all-methyl layer (*d*-space value of 8.8 Å) to a layer containing only *p*-aminobenzyl groups would predict *d* spacings of 29.3 Å (20.5 + 8.8) and 26.3 Å (17.5 + 8.8), for the protonated and deprotonated species, respectively, obviously incompatible with the experimental results.

The structural models proposed in Figure 9, on the other hand, are in near agreement with the experimental *d*-space values. The observed *d* spacing of 23.0 Å for the protonated compound is very close to the predicted value of 23.3 Å obtained from summing *d*-space values of the all-methyl and the $x = 0.5$ compounds. Analogously, the deprotonated, staged $x = 0.25$ system *d*-space value of 21.6 Å compares favorably to the theoretical value of 21.2 Å that results from adding the $x = 0.0$ and $x = 0.5$ experimental values. Such staged compounds, in which a layer of single-pendant-group derivatization is adjacent to a layer of mixed-pendant-group derivatization, represent a

(19) Deviation from Vegard's law may not be profound enough to warrant applying a new designation (for example LA law) to the observed behavior.

(20) Alberti, G.; Costantino, J.; Kornyei, J.; Giovagnotti, M. L. L. *React. Polym.* **1985**, *4*, 1.
(21) Clearfield, A.; Wang, J. D.; Tian, Y.; Stein, E.; Bhardwaj, C. *J. Solid State Chem.* **1995**, *117*, 275.
(22) Alberti, G. In *Solid-State Supramolecular Chemistry: Two- and Three-dimensional Inorganic Networks*; Alberti, G., Bein, T., Eds.; Comprehensive Supramolecular Chemistry, Vol. 7; Pergamon-Elsevier Science: Amsterdam, 1996; Chapter 5.

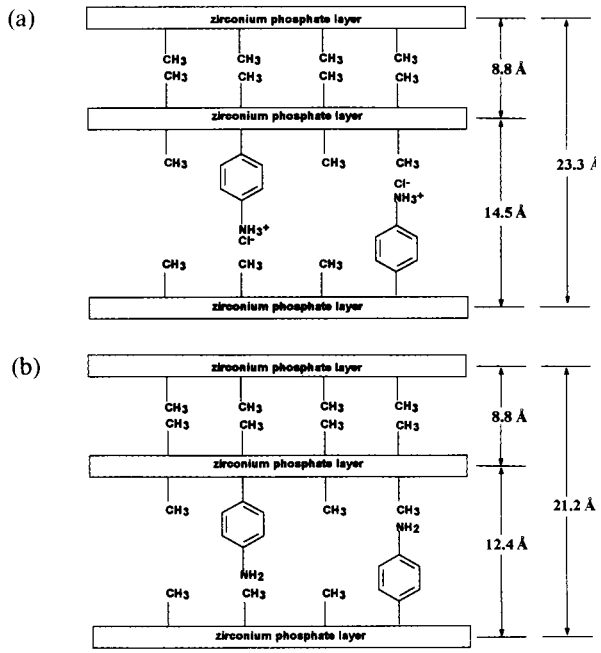

Figure 9. Models for the staged compounds (a) $Zr(pabHCl)_{0.25}(me)_{1.75}$ and (b) $Zr(pab)_{0.25}(me)_{1.75}$. Actual distances are discussed in the text.

novel class of zirconium phosphonate layered materials. A similar staging effect for the mixed phosphite−phosphate system was observed by Alberti et al.[23]

The second XRD peak, then, represents the true, mixed $x = 0.25$ compound. Its 2θ value falls almost exactly on the second order diffraction of the staged material; peak widths prevent any observable resolution.

Conclusions

In this work, two new series of mixed zirconium phosphonates, $Zr(pabHCl)_x(me)_{2-x}$ and $Zr(pab)_x(me)_{2-x}$, have been synthesized and characterized. Analytical measurements (TGA, IR, NMR) confirmed both qualitatively and quantitatively that the desired stoichiometries can be obtained.

Through XRD, it was found that the interlayer spacings of these layered compounds did steadily increase with additional large-group content. This correlation can best be described as a positive deviation from the previously hypothesized, ideal Vegard's law behavior. Such behavior is reminiscent of other physical properties of binary mixtures (e.g., Raoult's law).

The modeling calculations have shown that there is a consistent increase in *d*-space values for our systems of mixed-derivative compounds, as the large-group content in increased. This can be understood to result from an energy minimization with respect to the rotational degrees of freedom of (i) the anchoring $P-C(sp^3)$ bond and (ii) the plane of the aromatic ring. We fully expect that similar conformational adjustments are at work in mixed systems examined previously.[13,14] In these systems, however, the larger number of degrees of freedom in the movements of the butylcarboxy and the propylamine groups would prohibitively increase the complexity of the search for minimum-energy conformations.

A novel layered material was found to be produced at one of the stoichiometries. When $x = 0.25$, for both the protonated and deprotonated species, the compound possesses a staged, or segregated, structure. These systems represent the first instance where phosphonate layered materials contain, in alternating fashion, an interlayer region of one moiety and an interlayer region of two, randomly mixed groups. Our results point to the possibility of forming new materials where one type of layer can insulate neighboring ones in which properties may be adjusted for specific purposes.

Acknowledgment. We thank the University of Vermont for financial support of this work through UCRS Grant No. PSCI94-2 and for the acquisition of the MSI-Cerius[2] calculational software package through a Research Advisory Council grant.

IC980664Y

(23) Alberti, G.; Costantino, J.; Perego, G. *J. Solid State Chem.* **1986**, *63*, 455.